

BallGAN: 3D-aware Image Synthesis with a Spherical Background

Minjung Shin¹ Yunji Seo¹ Jeongmin Bae¹ Young Sun Choi¹
 Hyunsu Kim² Hyeran Byun¹ Youngjung Uh¹
 Yonsei University¹ NAVER AI Lab²

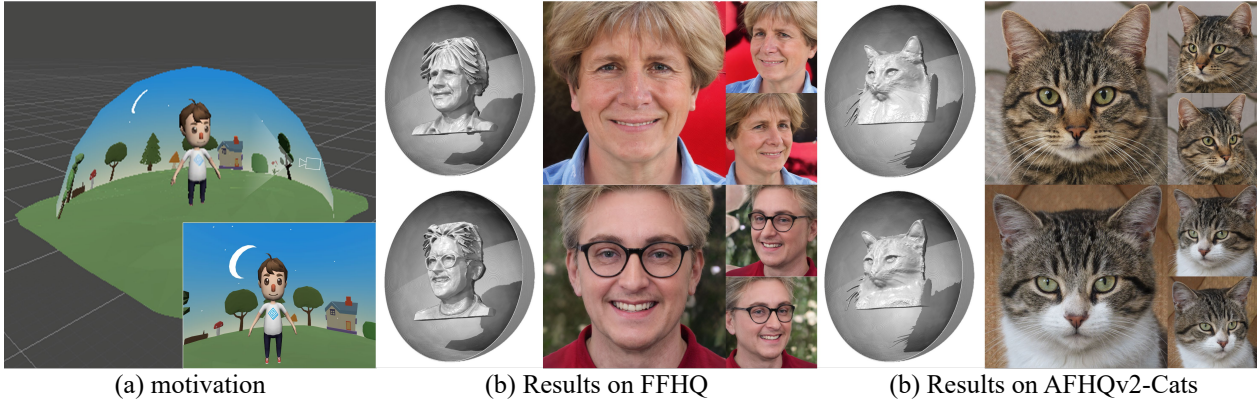


Figure 1. Our motivation (a), mesh visualization and result images of our method on FFHQ (b) and AFHQv2-Cat (c). We model the background with a spherical surface to resolve unnecessary depth ambiguity in the background.

Abstract

3D-aware GANs aim to synthesize realistic 3D scenes such that they can be rendered in arbitrary perspectives to produce images. Although previous methods produce realistic images, they suffer from unstable training or degenerate solutions where the 3D geometry is unnatural. We hypothesize that the 3D geometry is underdetermined due to the insufficient constraint, i.e., being classified as real image to the discriminator is not enough. To solve this problem, we propose to approximate the background as a spherical surface and represent a scene as a union of the foreground placed in the sphere and the thin spherical background. It reduces the degree of freedom in the background field. Accordingly, we modify the volume rendering equation and incorporate dedicated constraints to design a novel 3D-aware GAN framework named BallGAN. BallGAN has multiple advantages as follows. 1) It produces more reasonable 3D geometry; the images of a scene across different viewpoints have better photometric consistency and fidelity than the state-of-the-art methods. 2) The training becomes much more stable. 3) The foreground can be separately rendered on top of different arbitrary backgrounds. Project page: <https://minjung-s.github.io/ballgan/>

1. Introduction

Traditional generative adversarial networks (GANs) synthesize realistic images. Although they provide some control over the camera poses [11, 28–30], they lack explicit 3D understanding of the scenes. Recently, 3D-aware GANs [4, 21, 27, 39] reformulate the generative procedure as modeling the potential 3D scenes and rendering them to images. The state-of-the-art 3D-aware GANs [3, 10, 35] rely on neural radiance fields or their variants to represent 3D scenes. It is important to note that the generated 3D scenes become geometrically plausible even without 3D supervision or multi-view supervision, leading to realistic images with multi-view consistency across different perspectives.

The key challenge in 3D-aware GANs is to build a 3D model of the scene which will be rendered in the images. Generating 3D scene is a severely under-constrained problem compared to 3D reconstruction, or inverse rendering, which uses abundant supervisions such as multiple views in different perspectives or lighting conditions to settle the depth ambiguity. In other words, the 3D scene has excessive degree of freedom while the only constraint is producing realistic images guided by the discriminator. Although the rendered images are realistic, the image synthesis process conceal the degenerate solutions for the underlying 3D geometries, e.g., broken shapes and faces attached to walls as

shown in Figure 2 do not resemble the foreground geometry shown in the resulting images. Some methods try to circumvent the degenerate solutions by involving external guides such as prior knowledge [38] or off-the-shelf tools [18].

To solve this problem, we are inspired by a popular approach for video games or movies in the graphics community; representing salient objects with detailed 3D models and approximating peripheral scenery with simple surfaces (Figure 1(a)). It drastically reduces the complexity of scenes by devoting less resources to the background. As human vision system focus more on salient objects than the background, such technique does not degrade the user’s experience.

Accordingly, we represent a 3D scene as a union of a foreground and a surrounding spherical surface for the background as shown in Figure 2(d). The foreground is represented by the neural feature field with its density in continuous 3D space and the background is represented by an opaque neural feature field defined on the surface of a sphere. We also modify the volume rendering equation and incorporate dedicated constraints. Our formulation, named BallGAN, reduces the unnecessary degree of freedom and constrains the unbounded 3D background region to the 2D surface. In effect, our model greatly resolves degenerate solutions and improves on training stability, and produces realistic foreground 3D geometry.

Foreground-background separation of BallGAN is different from that of existing methods in the following aspects. GIRAFFE [23, 35] separates the latent space between foreground and background without reducing the solution space; the background receives the same range of coordinates as the foreground. StyleNeRF [10] restricts the background to be outside of the foreground but the background still has depth ambiguity in the 3D space. On the contrary, BallGAN inherently design a one-to-one mapping between a pixel and a background point which resolves the depth ambiguity problem.

Our model produces comparable or higher image quality on broad datasets (FFHQ, AFHQv2-Cats, and CompCars) and achieves state-of-the-art 3D-awareness considering the quality of the underlying 3D geometry and the multi-view consistency of the generated scenes. BallGAN clearly separates the foreground 3D object from the background without additional supervision or aid of off-the-shelf tools leading to convenient composition of the foreground object rendered in arbitrary perspectives on top of preferred backgrounds.

2. Related work

3D-aware GANs Generators in 3D-aware GANs involve representing 3D scenes somehow and rendering them to 2D images so that the generator is aware of the 3D scene given only a collection of unstructured 2D images. HoloGAN [21] represents a scene with a 3D grid of voxels con-

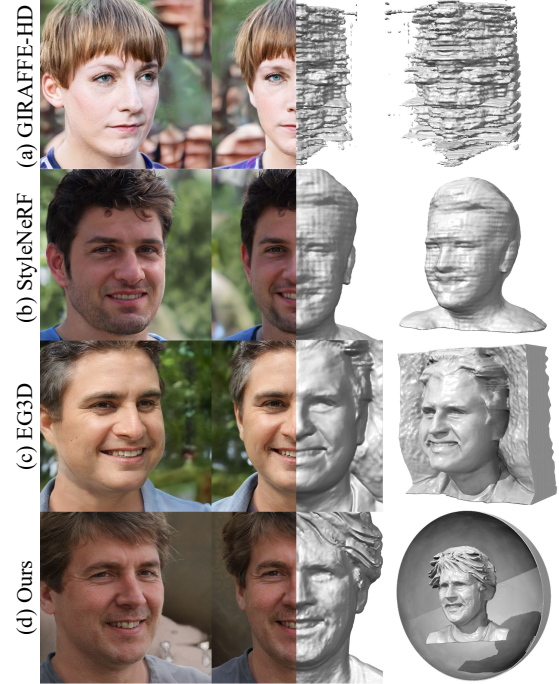
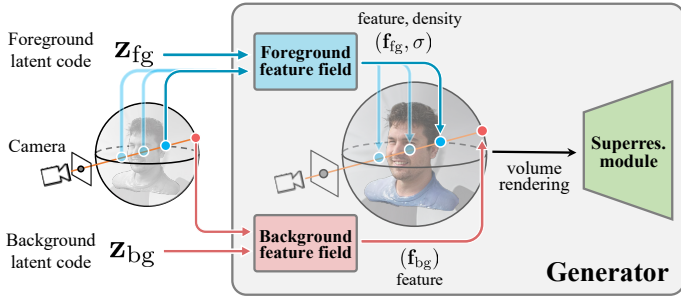


Figure 2. **Comparison of the 3D geometry extracted by marching cubes.** Previous methods exhibit degenerate solutions such as broken shape, jaggy surface, or sticking wall.

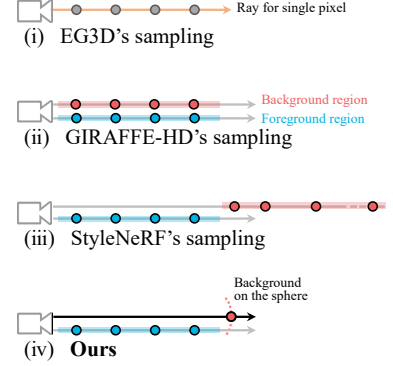
taining feature vectors, *i.e.*, 4D tensor. However, as 3D grid of voxels is limited by computational complexity, its maximum resolution is 128^2 .

Recent 3D-aware GANs integrate neural radiance fields (NeRFs) [20]. NeRFs represent a scene by a function of 3D coordinates producing RGB color and density at the location so that the scene can be projected onto images from arbitrary camera poses via volume rendering. It dramatically reduces the required memory and succeeds synthesizing 512^2 images [27]. Its successors improves image quality and 3D awareness by 1) enhancing the function for NeRF [4, 10], 2) volume rendering feature field followed by neural rendering with upsampling blocks [3, 10, 23, 33, 35], or 3) designing voxel-based [8, 12, 22, 32, 33]/hybrid [3] representations. Our method introduces a separate NeRF for modeling spherical background which encloses the foreground of EG3D [3] or StyleNeRF [10].

Scene decomposition Some methods decompose the 3D scenes into multiple components. GIRAFFE and its variant [23, 35] separate the objects and background so that the objects can be changed while the background is fixed. However, their background representation lives in the same ray points with the foregrounds and the 3D geometry does not benefit from the separation. StyleNeRF [10] separate the background outside a sphere following NeRF++ [37] where



(a) BallGAN Generator Overview



(b) Comparison of ray points

Figure 3. **Overview of the BallGAN generator and definition of ray points.** We bound the 3D space with an opaque background on a spherical surface. (i) EG3D does not separate the background. (ii) GIRAFFE-HD samples the background points within the same range of the foreground. (iii) StyleNeRF samples multiple background points outside the boundary. (iv) We sample a single background point on the sphere. It drastically reduces the depth ambiguity on the background.

the background region goes through the same volume rendering with multiple ray points at variable depth. On the contrary, we remove the depth ambiguity of the background by modeling it with an opaque representation on a 2D spherical surface enclosing the foreground.

3. BallGAN

In this section, we provide an overview of our framework and describe its key components and intuitions.

Overview BallGAN represents a 3D scene as a union of a usual foreground and a background on a spherical surface according to our intuition: approximating the unbounded background as a thin surface reduces the unnecessary degree of freedom of the scene.

As shown in Figure 3, our generator consists of two backbone networks for foreground and background (§3.1). Representations from these networks are rendered by our modified volume rendering equation to synthesize images (§3.2) and trained with GAN objectives and auxiliary regularizations (§3.3).

3.1. Bounding the 3D space

While traditional 2D GANs learn a function that maps random latent codes to arrays of RGB pixels in fixed dimensions, 3D-aware GANs aim to produce realistic images by synthesizing 3D scenes from random latent codes and rendering them into 2D images. In contrast to training NeRFs with multi-view observations of a single scene, the only objective for the 3D-aware GANs is producing realistic 2D images. I.e., the datasets do not provide any clues for the 3D geometry. Hence, training 3D-aware GANs is under-constrained problem and existing methods are prone to suf-

fer from the inherent depth ambiguity as shown in Figure 2.

To reformulate 3D-aware generation as an easier constrained problem, we represent the 3D scene as a union of two different representations for foreground and background: a foreground in a usual representation and a background on a thin opaque spherical surface. The spherical surface approximates the 3D space to a 2D coordinate system in which the depth ambiguity no more exists. It also covers the entire background for all possible camera viewpoints. We expect confining the background representation to allow the generator to focus on synthesizing more realistic foreground.

Background model We model the background as a neural feature field defined on a sphere with a fixed radius. Given a ray $\mathbf{r} = \mathbf{o} + t\mathbf{d}$ (t is the distance from the camera center \mathbf{o}), we find the 3D background point on the sphere with radius R_{bg} by simply computing the ray’s intersection on the sphere surface:

$$\mathbf{x}^{bg} = \mathbf{o} + \frac{-2[\mathbf{d} \cdot \mathbf{o}] + \sqrt{(2[\mathbf{d} \cdot \mathbf{o}])^2 - 4\|\mathbf{d}\|^2(\|\mathbf{o}\|^2 - R_{bg}^2)}}{2\|\mathbf{d}\|^2} \mathbf{d} \quad (1)$$

Since the background points are on a sphere surface of fixed radius R_{bg} , we further reparameterize the 3D coordinates \mathbf{x} as 2D spherical coordinates $\mathbf{s} = (\theta, \phi)$ leading to less computational complexity.

Then we represent the feature field F_{bg} using a StyleGAN2-like architecture :

$$F_{bg}(\mathbf{s}, \mathbf{z}_{bg}) = \mathbf{g}_{\mathbf{w}}^n \circ \dots \mathbf{g}_{\mathbf{w}}^1 \circ \zeta(\mathbf{s}), \quad (2)$$

where ζ is positional encoding [31] of \mathbf{s} , a mapping network

maps a noise vector \mathbf{z}_{bg} from the spherical Gaussian space \mathcal{Z} to the style space $\mathbf{w} \in \mathcal{W}$, and $\mathbf{g}_{\mathbf{w}}$ denotes 1×1 convolutions whose weights are modulated by \mathbf{w} . Note that there is no mapping for density from the background feature field because we our background is an opaque surface.

Our background representation drastically reduces the number of points to be fed to the model, *i.e.*, only one intersection of our sphere background and the ray \mathbf{r} . Therefore the hierarchical sampling is not required for the background.

Figure 3(b) visualizes the difference in space for each methods with ray points. Previous methods do not separate foreground from background or has infinite options for the optimization problem for background modeling in continuous space.

On the other hand, our method separates the foreground and background and bounds the background space to lie on a thin surface. This effectively constrains the solution space improves training stability and output quality.

Foreground model We adopt EG3D [3] for foreground modeling, where a random foreground code \mathbf{z}_{fg} is fed to StyleGAN2 [17] network to produce a tri-plane representation. Afterwards, a lightweight MLP outputs feature, color, and density from the tri-plane representation. Formally:

$$(\mathbf{f}_{\text{fg}}, \sigma) = F_{\text{fg}}(\mathbf{x}, \mathbf{z}_{\text{fg}}). \quad (3)$$

3.2. Volume rendering

Volume rendering aggregates the neural feature field along the rays through individual pixels to produce feature maps for a given camera pose. The conventional volume rendering computes the contribution for all points $\{\mathbf{x}_i\}$ sampled on a ray using the same equation $T(\mathbf{x}_i)(1 - \exp(-\sigma(\mathbf{x}_i)\delta(\mathbf{x}_i)))$, where T denotes transmittance, σ denotes density.

We modify the volume rendering equation to reflect the design of our background: a single point with full density:

$$\mathbf{f}(\mathbf{r}) = \sum_{i=1}^{N_{\text{fg}}} T_i(1 - \exp(-\sigma_i\delta_i))\mathbf{f}_i^{\text{fg}} + T^{\text{bg}}\mathbf{f}^{\text{bg}}, \quad (4)$$

where $\mathbf{f}(\mathbf{r})$ is an aggregated pixel feature along the ray \mathbf{r} , $T_i = \exp(\sum_{j=1}^{i-1} -\sigma_j\delta_j)$ denotes accumulated transmittance at \mathbf{x}_i , \mathbf{f}_i and σ_i are the feature and the density at \mathbf{x}_i from F_{fg} , and $\delta_i = t_{i+1} - t_i$ denotes the distance between adjacent points. Since the background point is considered opaque and proceeded by all foreground points, we define its contribution using only the transmittance $T^{\text{bg}} = \exp(\sum_{j=1}^{N_{\text{fg}}} -\sigma_j\delta_j)$. It is equivalent to placing an opaque background behind the scene in computer graphics techniques.

To synthesize high-resolution images, we employ 2D-CNN-based super-resolution module to upsample and refine

the feature maps to an RGB image as commonly done in recent methods [3, 10, 23, 35].

3.3. Training objectives

We use the non-saturating GAN loss \mathcal{L}_{adv} [9] and R1 regularization \mathcal{L}_{R1} [19]. Additionally, we use two regularization.

Foreground Density Loss To encourage better geometry quality, we use foreground regularization to prevent foreground density from diffusing. Similar to Mip-NeRF 360 [2], our foreground loss decreases the entropy of the foreground densities on the ray to locate foreground points in the area where the actual geometry is located.

$$\mathcal{L}_{\text{fg}} = \sum_{i,j} \mathbf{w}_i \mathbf{w}_j |t_i - t_j| + \frac{1}{3} \sum_i \mathbf{w}_i^2 \delta_i, \quad (5)$$

where $\delta_i = t_{i+1} - t_i$ is the distance between adjacent points and \mathbf{w} is the weight for aggregation after sigmoid function. This regularization is the integral of the weighted distance between all pairs of points on each ray.

Background Transmittance Loss To ensure a clear separation between foreground and background, we introduce new regularization on T^{bg} . The ray corresponding to foreground object in image should have high foreground density that makes T^{bg} close to 0, and thus the background feature should not affect to the aggregated pixel. In contrast, foreground density should be small enough to make T^{bg} close to 1 when the ray corresponds to background, so that the aggregated pixel feature should be the same as the background feature. Therefore, we induce the transmittance of the background to be binarized:

$$\mathcal{L}_{\text{bg}} = \sum \min(T^{\text{bg}}, 1 - T^{\text{bg}}). \quad (6)$$

The total loss function is then

$$\mathcal{L}_{\text{total}} = \mathcal{L}_{\text{adv}} + \lambda_{\text{R1}} \mathcal{L}_{\text{R1}} + \lambda_{\text{fg}} \mathcal{L}_{\text{fg}} + \lambda_{\text{bg}} \mathcal{L}_{\text{bg}}, \quad (7)$$

where λ_{R1} , λ_{fg} and λ_{bg} are hyperparameters. For an ablation study on these losses, please check the supplemental materials.

4. Experiments

In this section, we evaluate the effectiveness of BallGAN compared to the baselines regarding faithfulness of underlying 3D geometry in §4.1, separation of foreground in §4.2, training stability in §4.3, and image quality in §4.4. Implementation details are in Appendix A.

Datasets We validate our method on two front-facing datasets, FFHQ [16] and AFHQv2-Cats [5, 15], and one 360° dataset, CompCars [36]. FFHQ has 70K images of



Figure 4. **Images rendered on various camera poses.** Previous methods show distortions especially on extreme camera poses. In contrast, BallGAN synthesizes realistic and multi-view consistent images.

real human faces, and AFHQv2-Cats contains 5,558 images of cat faces. We resize the resolutions of these datasets to be 512^2 . CompCars contains 136K images of cars with various resolutions and aspect ratios. In CompCars dataset, we use a center cropping for each image and resize it to 256^2 .

Competitors For our main comparisons we use EG3D [3], StyleNeRF [10] and GIRAFFE-HD [35]. We include MVC-GAN [38], VolumeGAN [34] and StyleSDF [24] for quantitative comparisons.

4.1. Faithfulness of the underlying 3D geometry

It is essential for 3D-aware GANs to model correct 3D geometry of the scenes such that their rendered images on arbitrary camera poses are convincing views of real 3D scenes. Qualitative comparisons are followed by quantitative comparisons.

Qualitative comparison: generated scenes Figure 4 compares how each method renders *generated* scenes on different perspectives, expecting the images to have multi-view consistency and realism. The leftmost column provides meshes of the scene for reference. We notice severe distortions in GIRAFFE-HD and StyleNeRF when the camera rotates more than $\pm 60^\circ$ implying their spurious 3D geometry. This problem is evident in the marching cube results of GIRAFFE-HD, which separately models foreground and background but without their separate ranges. StyleNeRF produces rough geometry and camouflages de-

tailed shapes with color. Discussion on the missing backgrounds is deferred to §4.2.

Similarly, the rendered images of EG3D show distortions from $\pm 60^\circ$ angles, *e.g.*, the ears are truncated first and then the cheeks at $\pm 90^\circ$ angles. The mesh explains that the faces are engraved to a concave wall expanding from the ridge of the faces. Furthermore, although the meshes show greater detail compared to StyleNeRF, there are areas of disagreement between the underlying geometry and its rendered images, *e.g.*, the boundary between hair and forehead is fuzzy in the geometry, whereas it becomes clear after color rendering.

On the other hand, BallGAN synthesizes realistic and multi-view consistent images, even the exact side faces. It implies that the separate background on a sphere removes the depth ambiguity and does not interfere with the foreground object. Furthermore, we observe greater details on hair and whiskers. Appendix C provides more detailed comparisons.

Qualitative comparison: inversion of real images Figure 5 compares renderings and meshes of the same scenes through pivotal tuning inversion (PTI) [25] of *real* images from the training set. Although the image reconstructions of all methods are similar in target pose, the differences become more visible in different viewpoints and in their underlying 3D geometries. GIRAFFE-HD apparently produces geometry that least fits the rendered image and thus renders inconsistent images in different views. StyleNeRF captures only rough outline and placements in the geometry so that color makes the rendered scene be realistic. Especially, the mesh does not reveal beard and the boundary between hair and forehead. EG3D recovers realistic geometry that mostly fits the given image but the faces are stuck to a wall. Furthermore, the rendered images sometimes have a hallucination of the face on the background. On the other hand, BallGAN’s geometry faithfully encompasses the details shown in the images: wavy hair, sideburns, beard, eyebrows.

Quantitative results We quantitatively compare the underlying 3D model following the protocols in EG3D [3]. In Table 1, ID measures multi-view facial identity consis-

	FFHQ 512 ²		
	ID \uparrow	Pose \downarrow	Depth \downarrow
MVC-GAN	0.583	0.01363	0.1230
VolumeGAN	0.630	0.02501	0.0201
StyleSDF	0.501	0.00958	0.0161
EG3D	0.705	0.00733	0.1130
GIRAFFE-HD	0.687	0.06435	0.0583
StyleNeRF	0.643	0.01848	0.0131
BallGAN (ours)	0.738	0.00474	0.0089

Table 1. Quantitative evaluation on 3D geometry. We report identity consistency (ID), pose accuracy, and depth errors for FFHQ.

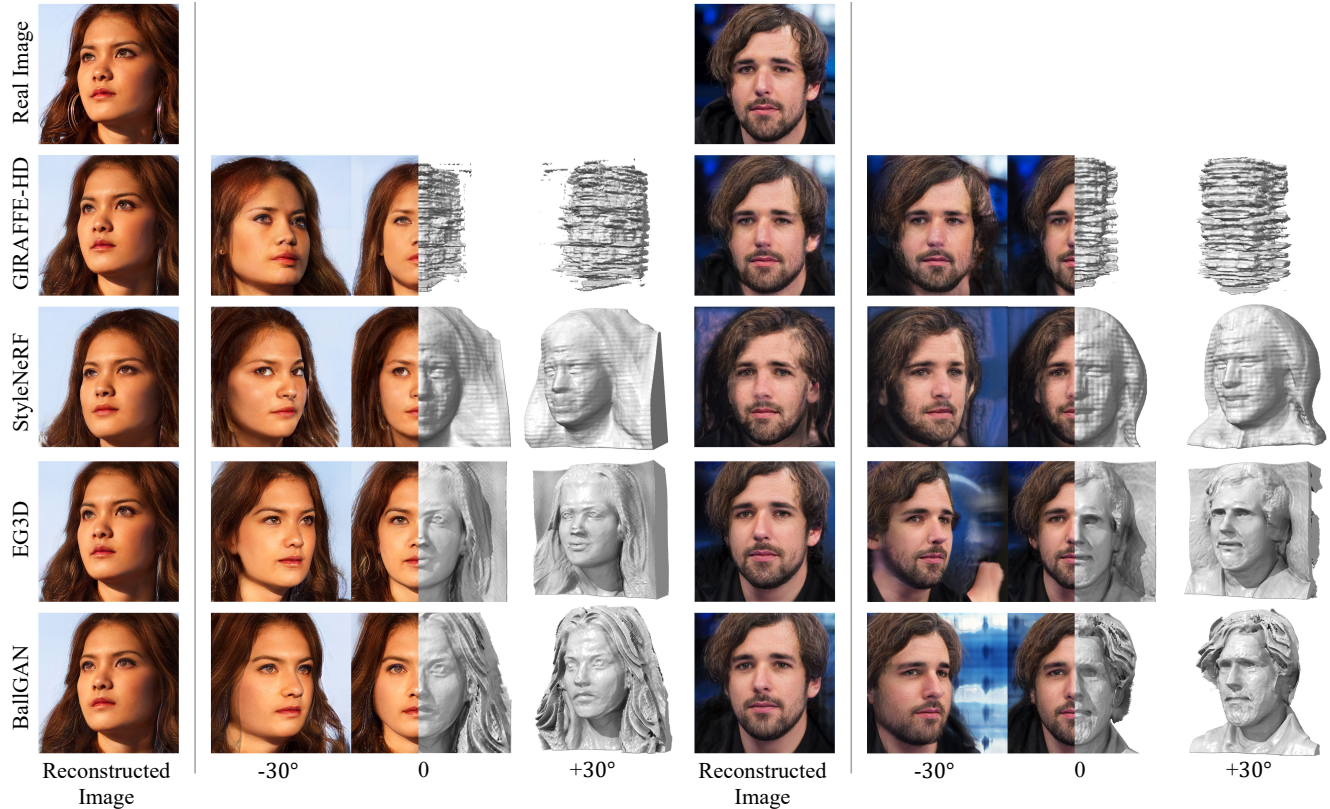


Figure 5. **Renderings and marching cubes of the same samples.** Although all methods similarly reconstruct the target real image by inversion, the underlying 3D geometries in the baselines are not realistic. On the other hand, BallGAN (ours) produces realistic shape including hair boundary. We adjusted the threshold for each mesh at the line where the pupils do not break.

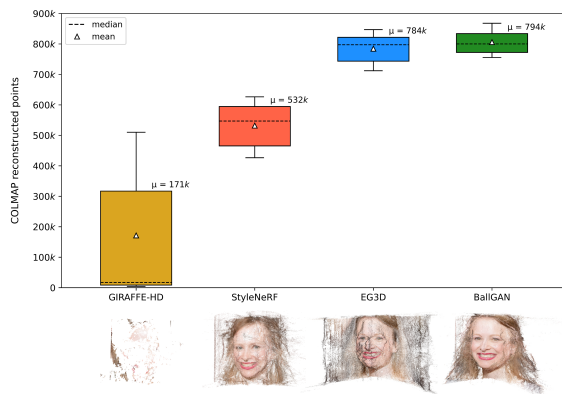


Figure 6. **COLMAP point cloud reconstruction** from 128 views in $[-\pi/2, \pi/2]$ of five scenes. More points indicate better multi-view consistency. The figure below is an example of COLMAP reconstruction.

tency¹, Depth indicates MSE of the expected depth maps

¹the mean Arcface [6] cosine similarity

from density against estimated depth-maps² in frontal view, and Pose implies controllability by MSE between the estimated pose of synthesized image and the input (target) pose. Appendix D describes further details of the protocol. BallGAN outperforms the baselines in all metrics.

We further push the evaluation: the number of reconstructed points from 128 views by COLMAP [26] in five inverted samples of FFHQ training set. Figure 6 provides the numbers and example point clouds of the methods. Since COLMAP reconstructs the points with high photometric consistency, the larger number of points indicates the higher multi-view consistency. We observe that BallGAN achieves the largest number of points closely followed by EG3D. However, large portion of the points from EG3D seats on the background walls rather than the face while ours densely lie on the faces.

4.2. Separated foregrounds

As the background on a spherical surface is one of the key component of our method, we evaluate the separabil-

²estimations for Depth and Pose are from [7]

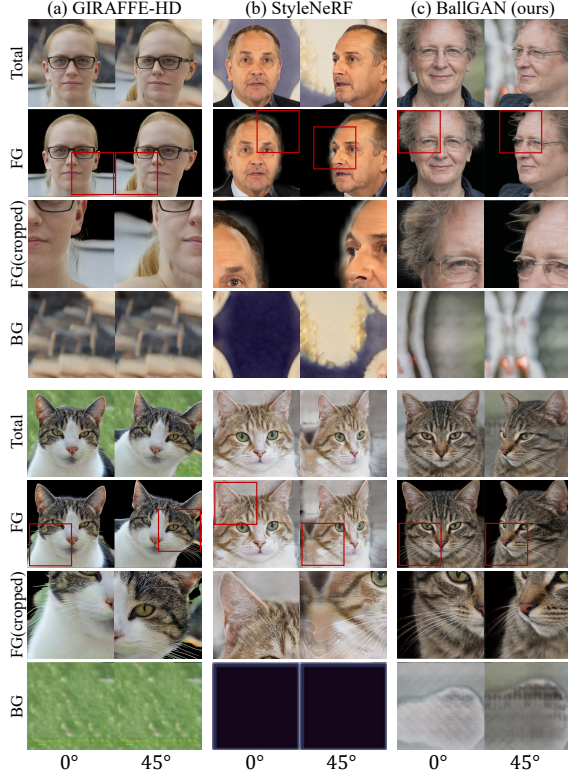


Figure 7. **Separate renderings of the foreground and background.** For easy comparison, we also show cropped foreground images. Our model can also separate details such as cat’s whiskers in the foreground.

ity and geometry of foregrounds against GIRAFFE-HD and StyleNeRF. Note that EG3D does not provide separation.

Qualitative comparison Figure 7 provides example rendered images. GIRAFFE-HD provides detailed separation on the images thanks to its auxiliary output, the alpha mask. However, the alpha mask comes from the 2D feature maps rather than the density in the 3D space, thus it often covers the background. Furthermore, the foregrounds are not consistent across different viewpoints. StyleNeRF shows better multi-view consistency but its foreground separation is less accurate on FFHQ, and shows no separation on AFHQv2-Cats. On the contrary, ours results show both fine separation and multi-view consistency.

User study In addition, we asked 57 participants to choose the best model in terms of foreground separation and consistency. Figure 8 shows that ours outperforms competitors by a large margin with respect to both criteria. See Appendix E for how we prepared images and questions for the user study.

Application Figure 9 demonstrates usecases of BallGAN. Given a real image, its inversion on BallGAN provides 3D

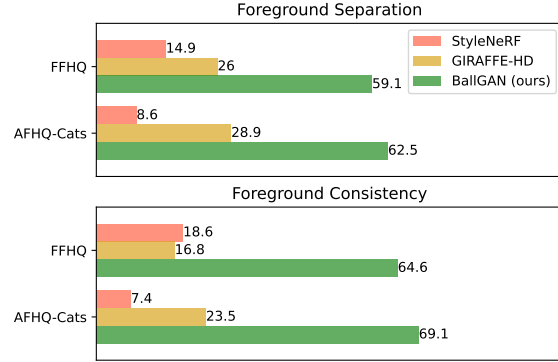


Figure 8. **User study.** Majority of participants prefer our method to the others on both foreground separation and consistency.

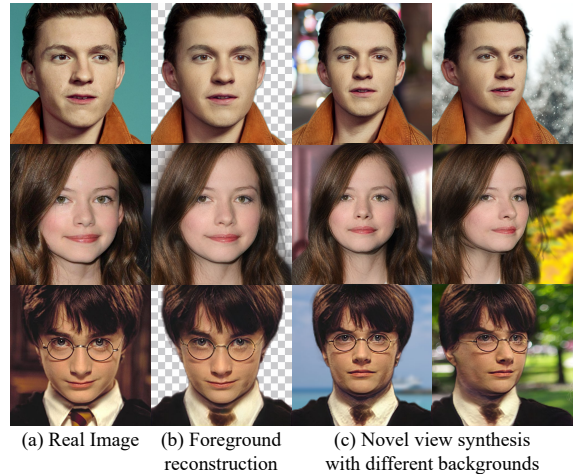


Figure 9. **Compositing foreground in different viewpoints on arbitrary backgrounds.** (a) is a target image, and (b) is a reconstructed foreground of ours using PTL. (c) is a result of novel views on arbitrary backgrounds. By changing the camera pose and FOV, we show that our model can generate attributes of unobserved regions well.

foreground that can be rendered in novel views and combined with different backgrounds. The alpha channel for the background is computed from the background transmittance in the volume rendering step, i.e., the last term in (4). Even the facial regions that are not seen in the original images are realistic in the rendered images such as chin. Note that Figure 9(c) has wider field-of-view than the standard to produce more natural results.

4.3. Training stability

Here, we demonstrate the effectiveness of applying BallGAN on StyleNeRF, namely BallGAN-S, using the CompCars dataset where EG3D is not applicable due to the ab-

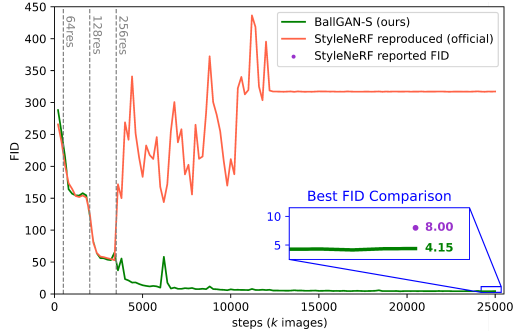


Figure 10. **FID graph of CompCars 256²**. FID for StyleNeRF reproduction flattens after 12,200 steps as gradient for the generator falls to zero after gradient explosion. In contrast BallGAN-S FID steadily converges below the reported FID of StyleNeRF.

Sep. FG/BG		FFHQ 512 ²	AFHQv2-Cats 512 ²	CompCars 256 ²
✗	MVCGAN	13.4 [†]	26.57 [‡]	-
	VolumeGAN	15.74	44.55	12.9 [†]
	StyleSDF	19.56	19.44	-
	EG3D	4.7[†]	2.77[†]	N/A
✓	GIRAFFE-HD	6.47	7.33	<u>7.1[‡]</u>
	StyleNeRF	10.51 [‡]	21.56	8 (284±96)
	BallGAN (ours)	<u>5.98</u>	<u>4.72</u>	4.26

Table 2. Quantitative comparison using FID on three datasets. [†] denotes the reported FID, and [‡] denotes the FID calculated by official checkpoint. In the case of StyleNeRF on CompCars, we report FID of diverged models. In the parenthesis, is the mean and standard deviation over 3 experiments. Our model is state-of-the-art among models on foreground background separation. Bold and underline indicate the best and second-best performance.

sence of camera pose estimator.

Figure 10 compares image quality of BallGAN-S and StyleNeRF using Fréchet Inception Distance (FID) [13] over iterations. While StyleNeRF diverges as the image resolution grows from 128² to 256²³, BallGAN-S smoothly converges below the reported FID of StyleNeRF. It implies that our method is generally beneficial to different foreground backbones and greatly improves training stability.

4.4. Evaluation on image quality

We evaluate generated image quality on the FFHQ 512², AFHQv2-Cats 512², CompCars 256² datasets. Images for FFHQ 512², AFHQv2-Cats 512² are generated by BallGAN and images for CompCars 256² are generated by BallGAN-S.

Quantitative results Table 2 compares image quality in FID.

For FFHQ, AFHQv2-Cats, BallGAN outperforms all the baselines except EG3D. Although EG3D achieves the

³This phenomenon is also reported in the official repository.

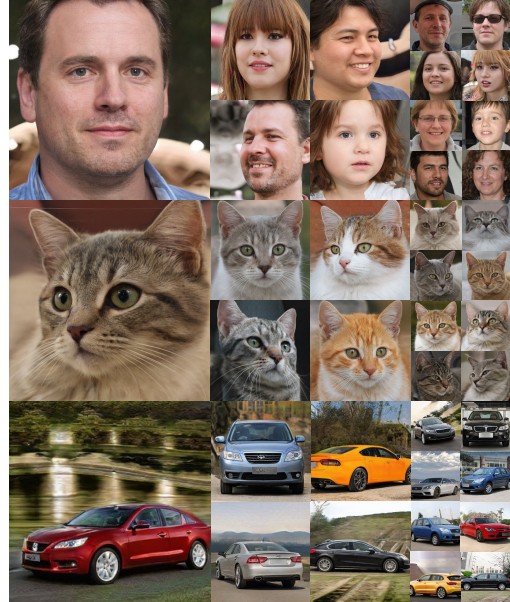


Figure 11. **Set of images generated by BallGAN**. We sample images of 512² resolution produced by BallGAN on FFHQ 512², AFHQv2-Cats 512² and CompCars 256². Each image is rendered with randomly sampled camera pose.

best FID, it suffers in generating 3D geometry (§4.1) and does not support foreground-background separation. Furthermore, EG3D requires camera poses of the real images which are not always available, e.g., CompCars. On the other hand, we achieve the state-of-the-art FID on CompCars with BallGAN-S and the second-best FID on FFHQ and AFHQv2-Cats closely following EG3D. We note that CompCars has more complex backgrounds and 360° camera poses.

Qualitative results Figure 11 provides example images generated by BallGAN and BallGAN-S. Our models faithfully generate diverse samples in multiple views. More examples can be found in Appendix F.

5. Conclusion

We have proposed a 3D-aware GAN framework, named BallGAN, regarding a scene as a 3D volume within a spherical surface so that the background representation lies on a 2D coordinate system. It relieves the depth ambiguity in the background and enhances the quality of 3D geometry in the foreground and training stability. Extensive experiments support superiority of our method compared to existing methods. BallGAN allows a useful application: rendering the foregrounds in arbitrary viewpoints on top of given backgrounds.

Supplementary Materials for BallGAN

Minjung Shin¹ Yunji Seo¹ Jeongmin Bae¹ Young Sun Choi¹
 Hyunsu Kim² Hyeran Byun¹ Youngjung Uh¹
 Yonsei University¹ NAVER AI Lab²

We provide the following supplementary materials:

- A Implementation details
- B Ablation of the losses
- C Detailed multi-view comparison
- D Evaluation protocols
- E User study details
- F Uncurated samples

A. Implementation details

BallGAN Our implementation mostly follows the official implementation of EG3D¹ including training hyperparameters, two-stage training, equalized learning rates [14], a mini-batch standard deviation layer at the end of the discriminator [14], exponential moving average of the generator weights, a non-saturating logistic loss [9], and R1 regularization [19] with $\gamma = 1$. We also use the same camera intrinsic parameters and FFHQ preprocessing from EG3D.

The weights of the last layer for the density are initialized to zero to guarantee the contribution of the background at the beginning of the training. Figure S1 illustrates the architecture for the background representation. A five-layer 1×1 convolutional network maps the positional encoding ζ of a background point to a feature vector. The style code from an eight-layer MLP, *i.e.*, the mapping network, modulates the weights of the convolutions $\mathbf{g}_{\mathbf{w}_{\text{bg}}}$. The background representation mapping network shares the same design as the mapping network in StyleGAN2 [17]. The number of channels of the intermediate features are in Table S1. The last layer has a sigmoid clamping from MipNeRF [1] as in the foreground neural render of EG3D. We use the positional encoding for the background following StyleNeRF [10] with $L = 10$ without viewing direction.

On FFHQ, we schedule the coefficient of the foreground density loss λ_{fg} to exponentially grow from 0 to 0.25 and the coefficient of the background transmittance regularization λ_{bg} to exponentially grow from 0 to 1 in the first stage. We set the coefficients $\lambda_{\text{fg}} = 0$ and $\lambda_{\text{bg}} = 0.05$ in the second stage.

For AFHQv2-Cats, we start from the weights pretrained

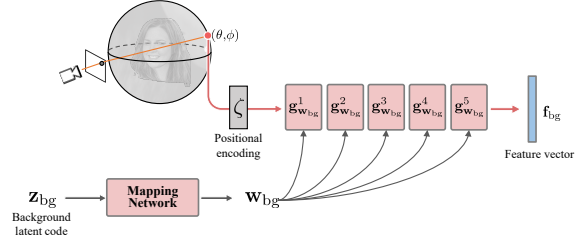


Figure S1. Background architecture

	input channel	output channel
PE	2	40
$\mathbf{g}_{\mathbf{w}_{\text{bg}}}^1$	40	64
$\mathbf{g}_{\mathbf{w}_{\text{bg}}}^2$	64	64
$\mathbf{g}_{\mathbf{w}_{\text{bg}}}^3$	64	64
$\mathbf{g}_{\mathbf{w}_{\text{bg}}}^4$	64	64
$\mathbf{g}_{\mathbf{w}_{\text{bg}}}^5$	64	32

Table S1. Detail of background representation. PE means positional encoding ζ , not a layer.

on FFHQ for the first step and fine-tune them on AFHQv2-Cats as done in EG3D. We set $\lambda_{\text{fg}} = \lambda_{\text{bg}} = 0$ to let the foreground better capture the fine details such as whiskers.

BallGAN-S BallGAN-S is a variant using StyleNeRF as a baseline instead of EG3D. We add the same background network on top of the official StyleNeRF implementation². We set $\lambda_{\text{fg}} = 0.25$ and $\lambda_{\text{bg}} = 0$.

Competitors Table 2 shows the best FIDs among the available sources: reported, official checkpoints, and official training code. We used the official training codes as-is to reproduce FIDs if the official repository does not provide the checkpoints^{3,4,5}. For GIRAFFE-HD on CompCars, we applied transfer-learning from the official checkpoint for 256² resolution to 512² resolution following the authors’

²<https://github.com/facebookresearch/StyleNeRF>

³<https://github.com/genforce/volumegan>

⁴<https://github.com/royorel/StyleSDF>

⁵<https://github.com/AustinXY/GIRAFFEHD>

¹<https://github.com/NVlabs/eg3d>

	reported	FFHQ 512 ² reproduced	official ckpt.	FFHQ other res. reported
GRAM	-	-	-	(256 ²) 29.8
MVCGAN	13.4	-	21.3	
VolumeGAN	-	15.7	-	(256 ²) 9.1
StyleSDF	-	19.5	-	(256 ²) 11.5
EG3D	4.7	4.7	-	
GIRAFFE-HD	-	6.4	-	(1024 ²) 10.13
StyleNeRF	13.2	-	10.5	
Ours	5.98			

Table S2. **FIDs of competitors from various sources.** We report the best fid among the reported, reproduced and official checkpoint for each model with 512² resolutions in Table 2.

	configuration		
	\mathcal{L}_{fg}	\mathcal{L}_{bg}	FID
stage 1	-	-	7.87
	✓	-	6.82
	-	✓	7.88
	✓	✓	6.13
stage 2	-	-	6.01

Table S3. **Ablation study on regularization.** This ablation study is conducted with batch size 16 due to the resource shortage.

guidelines. We trained the model until it achieved the FID reported in the original paper. Table S2 provides the FIDs we obtained from various sources.

B. Ablation of the losses

We conduct ablation studies to evaluate the effect of each regularization. Table S3 shows the effects of our foreground and background regularization. Applying foreground density loss \mathcal{L}_{fg} improves the image quality. Additionally using background regularization \mathcal{L}_{bg} , we get the best image quality. This is because, the background transmittance loss \mathcal{L}_{bg} encourages the foreground density to either completely block or leave the space empty before the rays hit the background, *i.e.*, produces clear separation between foreground and background. Figure S2 shows examples where the background is and is not fully occluded by the foreground, as a result of removing or using the background transmittance loss \mathcal{L}_{bg} . Note that the ablation study is conducted with a batch size of 16 due to the resource shortage. Therefore the full FID is higher than our final FID of 5.98 produced with a batch size of 32.

C. Detailed multi-view comparison

Figure S3a and Figure S3b provide qualitative comparisons with varying camera poses. As FFHQ dataset mainly consists of frontal view, the competitors produce artifacts or inconsistency. On the other hand, BallGAN produces images that are multi-view consistent and free from artifacts even in extreme camera poses.

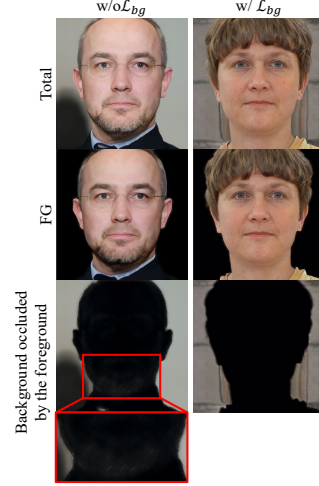


Figure S2. **Visual comparison on the effect of BG regularization.** We generate two samples with the same seed. Left column is image generated with bg regularization and the right column is image generated without bg regularization. They are both outputs from the first stage of training as mentioned in §A.

D. Evaluation protocols

We mostly follow EG3D [3].

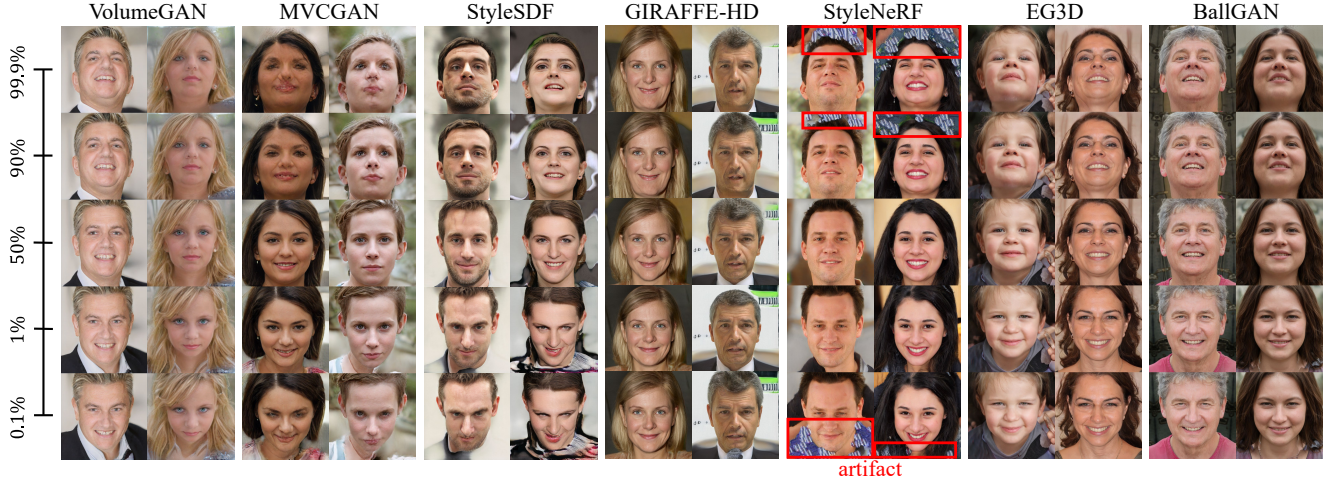
Real image inversion We use the same configuration for pivotal tuning inversion [25] and the number of iterations.

ID ID measures the difference between the different views of the same scene. For each method, we generate 1000 random scenes in pairs of randomly selected poses from the training dataset pose distribution. For each sample pair, we measure the ArcFace [6] cosine similarity and compute the average.

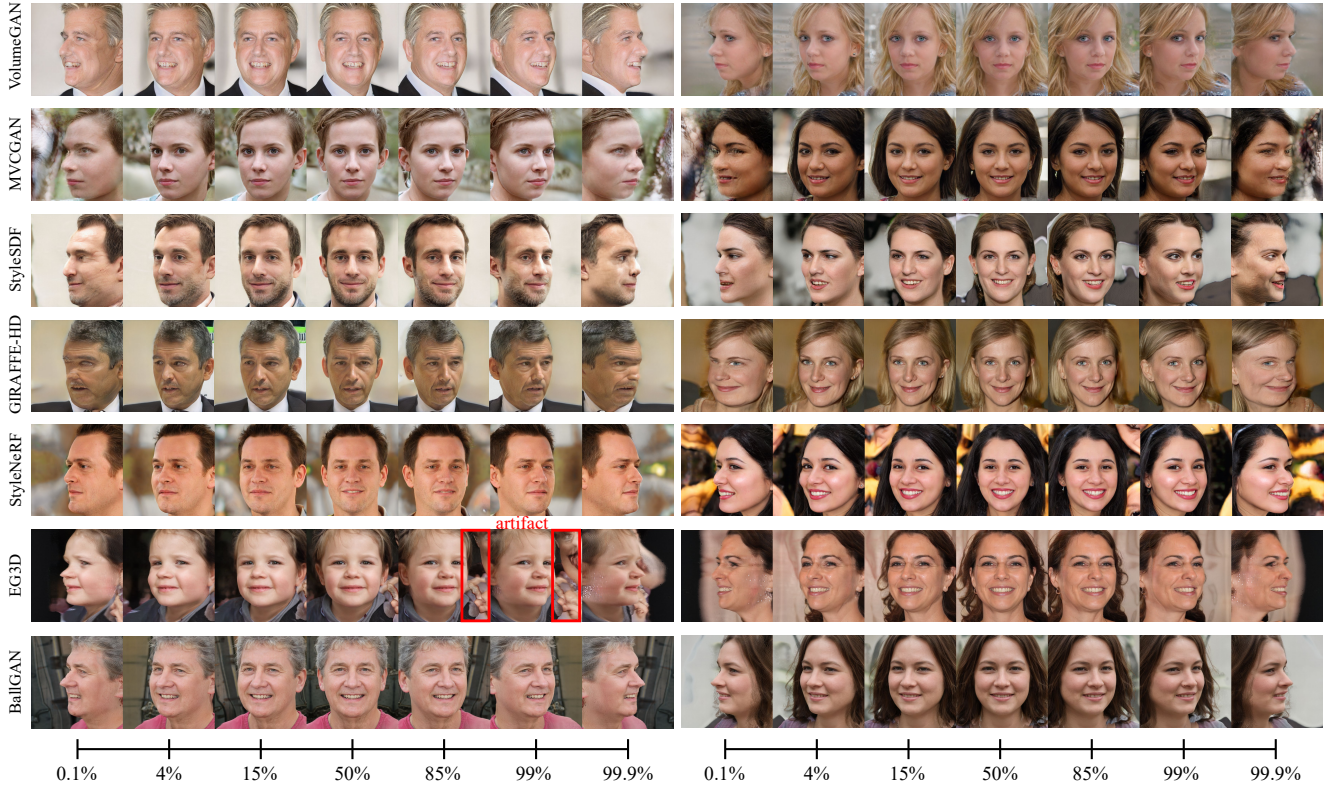
Pose Pose computes the difference between the intended pose and the synthesized pose implying the pose controllability. We sample 1000 latent codes and render them in varying yaws and estimate the resulting yaws with a pre-trained face reconstruction model [7]. Instead of random yaws, we remove stochasticity by specifying nine yaw angles evenly separated in $[-0.9\text{rad}, 0.9\text{rad}]$. $\pm 0.9\text{rad}$ covers the [0.3, 99.7] percentile of training dataset’s yaw distribution. We report mean absolute error (L1) instead of L2 distance to better capture the error near zero.

Depth Depth measures the difference between the underlying 3D geometry (volume-rendered depth) and the rendered image. We consider depth maps of rendered images in frontal views of 1000 samples estimated by a pre-trained 3D face reconstruction model [7] as pseudo ground-truth. The depth maps are normalized to compute their mean squared error.

Foreground separation We describe the procedure to obtain the foreground image used in §4.2. Please note that al-



(a) Multi-view comparison with varying pitches



(b) Multi-view comparison with varying yaws

Figure S3. **Multi-view comparison in various poses on FFHQ.** Percentile for camera pitch and yaw in training distribution are shown on the left (a) and below (b).

though our goal is to compare the separation of foreground and background in the 3D space, it is prohibitive to visualize the 3D space in the paper or screen. Therefore, we visualize by separately synthesizing the foreground scene for each method. However, GIRAFFE-HD has foreground densities only in the central region of the image canvas and their aggregated densities do not match the shape of the

salient object. In StyleNeRF, the aggregation of the foreground densities along the ray does not reach one, *i.e.*, the foreground is semi-transparent. Hence, we used the alpha masks from GIRAFFE-HD’s refine renderer. For StyleNeRF, we searched for the threshold that best fits the foreground region for each image. Ours do not require such workarounds as the foreground densities aggregates to one

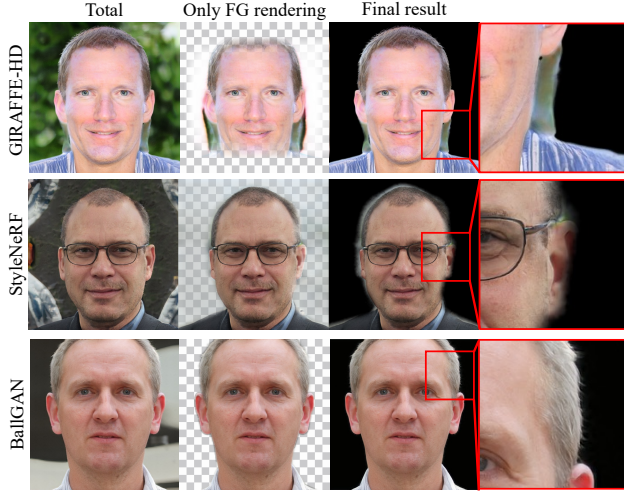


Figure S4. **Foreground separation examples.** The densities along a ray do not sum to one in GIRAFFE-HD and StyleNeRF. Hence, we apply postprocessing to exploit their full potential for separation. Ours does not require such postprocessing.

along a ray. Figure S4 provides examples.

E. User study details

We prepared the following questionnaire for our user study in Figure 8. We randomly sampled ten scenes from each method and rendered them in seven different viewing directions. Then we asked 57 participants to answer two questions: (1) Which set of foreground includes the whole person and excludes the background? (2) Which set of foregrounds are consistent across different views?

F. Uncurated samples

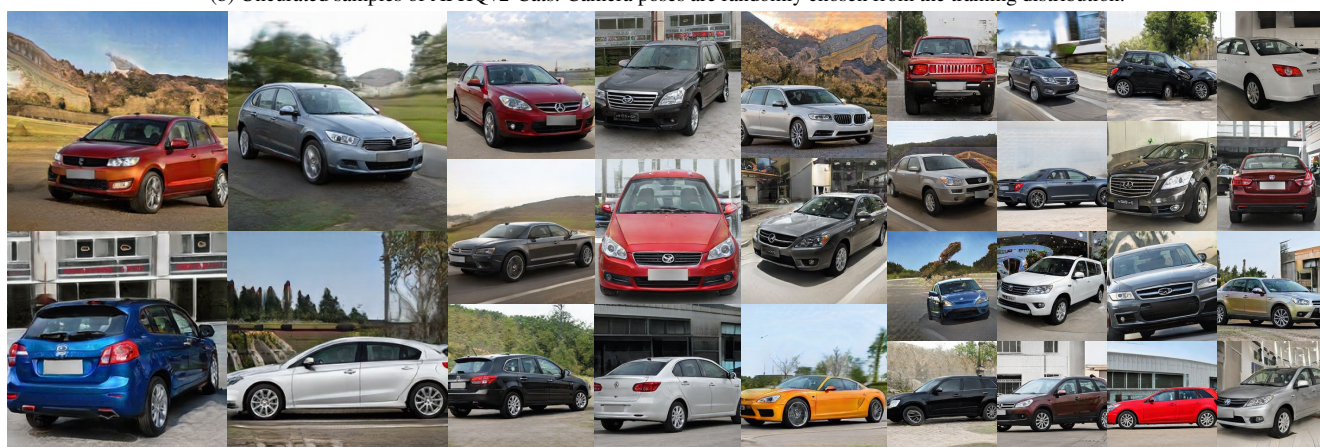
Figure S5 provides uncurated samples of our method.



(a) Uncurated samples of FFHQ. Camera poses are randomly chosen from the training distribution.



(b) Uncurated samples of AFHQv2-Cats. Camera poses are randomly chosen from the training distribution.



(c) Uncurated samples of CompCars. Camera poses are randomly chosen from the training distribution.

Figure S5. **Uncurated samples on the FFHQ, AFHQv2-Cats, and CompCars.** (a) and (b) show outputs of BallGAN. (c) is outputs from BallGAN-S.

References

- [1] Jonathan T Barron, Ben Mildenhall, Matthew Tancik, Peter Hedman, Ricardo Martin-Brualla, and Pratul P Srinivasan. Mip-nerf: A multiscale representation for anti-aliasing neural radiance fields. In *Proceedings of the IEEE/CVF International Conference on Computer Vision*, pages 5855–5864, 2021. 9
- [2] Jonathan T Barron, Ben Mildenhall, Dor Verbin, Pratul P Srinivasan, and Peter Hedman. Mip-nerf 360: Unbounded anti-aliased neural radiance fields. In *Proceedings of the IEEE/CVF Conference on Computer Vision and Pattern Recognition*, pages 5470–5479, 2022. 4
- [3] Eric R Chan, Connor Z Lin, Matthew A Chan, Koki Nagano, Boxiao Pan, Shalini De Mello, Orazio Gallo, Leonidas J Guibas, Jonathan Tremblay, Sameh Khamis, et al. Efficient geometry-aware 3d generative adversarial networks. In *Proceedings of the IEEE/CVF Conference on Computer Vision and Pattern Recognition*, pages 16123–16133, 2022. 1, 2, 4, 5, 10
- [4] Eric R Chan, Marco Monteiro, Petr Kellnhofer, Jiajun Wu, and Gordon Wetzstein. pi-gan: Periodic implicit generative adversarial networks for 3d-aware image synthesis. In *Proceedings of the IEEE/CVF conference on computer vision and pattern recognition*, pages 5799–5809, 2021. 1, 2
- [5] Yunjey Choi, Youngjung Uh, Jaejun Yoo, and Jung-Woo Ha. Stargan v2: Diverse image synthesis for multiple domains. In *Proceedings of the IEEE/CVF Conference on Computer Vision and Pattern Recognition (CVPR)*, June 2020. 4
- [6] Jiankang Deng, Jia Guo, Niannan Xue, and Stefanos Zafeiriou. Arcface: Additive angular margin loss for deep face recognition. In *Proceedings of the IEEE/CVF conference on computer vision and pattern recognition*, pages 4690–4699, 2019. 6, 10
- [7] Yu Deng, Jiaolong Yang, Sicheng Xu, Dong Chen, Yunde Jia, and Xin Tong. Accurate 3d face reconstruction with weakly-supervised learning: From single image to image set. In *Proceedings of the IEEE/CVF Conference on Computer Vision and Pattern Recognition Workshops*, pages 0–0, 2019. 6, 10
- [8] Matheus Gadelha, Subhransu Maji, and Rui Wang. 3d shape induction from 2d views of multiple objects. In *2017 International Conference on 3D Vision (3DV)*, pages 402–411. IEEE, 2017. 2
- [9] Ian Goodfellow, Jean Pouget-Abadie, Mehdi Mirza, Bing Xu, David Warde-Farley, Sherjil Ozair, Aaron Courville, and Yoshua Bengio. Generative adversarial nets. *Advances in neural information processing systems*, 27, 2014. 4, 9
- [10] Jiatao Gu, Lingjie Liu, Peng Wang, and Christian Theobalt. Stylenerf: A style-based 3d-aware generator for high-resolution image synthesis. *arXiv preprint arXiv:2110.08985*, 2021. 1, 2, 4, 5, 9
- [11] Erik Härkönen, Aaron Hertzmann, Jaakko Lehtinen, and Sylvain Paris. Ganspace: Discovering interpretable gan controls. *Advances in Neural Information Processing Systems*, 33:9841–9850, 2020. 1
- [12] Philipp Henzler, Niloy J Mitra, and Tobias Ritschel. Escaping plato’s cave: 3d shape from adversarial rendering. In *Proceedings of the IEEE/CVF International Conference on Computer Vision*, pages 9984–9993, 2019. 2
- [13] Martin Heusel, Hubert Ramsauer, Thomas Unterthiner, Bernhard Nessler, and Sepp Hochreiter. Gans trained by a two time-scale update rule converge to a local nash equilibrium. *Advances in neural information processing systems*, 30, 2017. 8
- [14] Tero Karras, Timo Aila, Samuli Laine, and Jaakko Lehtinen. Progressive growing of gans for improved quality, stability, and variation. In *International Conference on Learning Representations*, 2018. 9
- [15] Tero Karras, Miika Aittala, Samuli Laine, Erik Härkönen, Janne Hellsten, Jaakko Lehtinen, and Timo Aila. Alias-free generative adversarial networks. *Advances in Neural Information Processing Systems*, 34:852–863, 2021. 4
- [16] Tero Karras, Samuli Laine, and Timo Aila. A style-based generator architecture for generative adversarial networks. In *Proceedings of the IEEE/CVF conference on computer vision and pattern recognition*, pages 4401–4410, 2019. 4
- [17] Tero Karras, Samuli Laine, Miika Aittala, Janne Hellsten, Jaakko Lehtinen, and Timo Aila. Analyzing and improving the image quality of StyleGAN. In *Proc. CVPR*, 2020. 4, 9
- [18] Yidi Li, Yiqun Wang, Zhengda Lu, and Jun Xiao. Depthgan: Gan-based depth generation of indoor scenes from semantic layouts. *arXiv preprint arXiv:2203.11453*, 2022. 2
- [19] Lars Mescheder, Andreas Geiger, and Sebastian Nowozin. Which training methods for gans do actually converge? In *International conference on machine learning*, pages 3481–3490. PMLR, 2018. 4, 9
- [20] Ben Mildenhall, Pratul P Srinivasan, Matthew Tancik, Jonathan T Barron, Ravi Ramamoorthi, and Ren Ng. Nerf: Representing scenes as neural radiance fields for view synthesis. In *European conference on computer vision*, pages 405–421. Springer, 2020. 2
- [21] Thu Nguyen-Phuoc, Chuan Li, Lucas Theis, Christian Richardt, and Yong-Liang Yang. Hologan: Unsupervised learning of 3d representations from natural images. In *Proceedings of the IEEE/CVF International Conference on Computer Vision*, pages 7588–7597, 2019. 1, 2
- [22] Thu H Nguyen-Phuoc, Christian Richardt, Long Mai, Yongliang Yang, and Niloy Mitra. Blockgan: Learning 3d object-aware scene representations from unlabelled images. *Advances in Neural Information Processing Systems*, 33:6767–6778, 2020. 2
- [23] Michael Niemeyer and Andreas Geiger. Giraffe: Representing scenes as compositional generative neural feature fields. In *Proceedings of the IEEE/CVF Conference on Computer Vision and Pattern Recognition*, pages 11453–11464, 2021. 2, 4
- [24] Roy Or-El, Xuan Luo, Mengyi Shan, Eli Shechtman, Jeong Joon Park, and Ira Kemelmacher-Shlizerman. StyleSDF: High-Resolution 3D-Consistent Image and Geometry Generation. In *Proceedings of the IEEE/CVF Conference on Computer Vision and Pattern Recognition (CVPR)*, pages 13503–13513, June 2022. 5
- [25] Daniel Roich, Ron Mokady, Amit H Bermano, and Daniel Cohen-Or. Pivotal tuning for latent-based editing of real im-

- ages. *ACM Transactions on Graphics (TOG)*, 42(1):1–13, 2022. 5, 10
- [26] Johannes L Schonberger and Jan-Michael Frahm. Structure-from-motion revisited. In *Proceedings of the IEEE conference on computer vision and pattern recognition*, pages 4104–4113, 2016. 6
- [27] Katja Schwarz, Yiyi Liao, Michael Niemeyer, and Andreas Geiger. Graf: Generative radiance fields for 3d-aware image synthesis. *Advances in Neural Information Processing Systems*, 33:20154–20166, 2020. 1, 2
- [28] Yujun Shen, Jinjin Gu, Xiaoou Tang, and Bolei Zhou. Interpreting the latent space of gans for semantic face editing. In *Proceedings of the IEEE/CVF conference on computer vision and pattern recognition*, pages 9243–9252, 2020. 1
- [29] Yujun Shen and Bolei Zhou. Closed-form factorization of latent semantics in gans. In *Proceedings of the IEEE/CVF Conference on Computer Vision and Pattern Recognition*, pages 1532–1540, 2021. 1
- [30] Alon Shoshan, Nadav Bhonker, Igor Kviatkovsky, and Gerard Medioni. Gan-control: Explicitly controllable gans. In *Proceedings of the IEEE/CVF International Conference on Computer Vision*, pages 14083–14093, 2021. 1
- [31] Matthew Tancik, Pratul Srinivasan, Ben Mildenhall, Sara Fridovich-Keil, Nithin Raghavan, Utkarsh Singhal, Ravi Ramamoorthi, Jonathan Barron, and Ren Ng. Fourier features let networks learn high frequency functions in low dimensional domains. *Advances in Neural Information Processing Systems*, 33:7537–7547, 2020. 3
- [32] Jiajun Wu, Chengkai Zhang, Tianfan Xue, Bill Freeman, and Josh Tenenbaum. Learning a probabilistic latent space of object shapes via 3d generative-adversarial modeling. *Advances in neural information processing systems*, 29, 2016. 2
- [33] Yinghao Xu, Sida Peng, Ceyuan Yang, Yujun Shen, and Bolei Zhou. 3d-aware image synthesis via learning structural and textural representations. In *Proceedings of the IEEE/CVF Conference on Computer Vision and Pattern Recognition*, pages 18430–18439, 2022. 2
- [34] Yinghao Xu, Sida Peng, Ceyuan Yang, Yujun Shen, and Bolei Zhou. 3d-aware image synthesis via learning structural and textural representations. In *CVPR*, 2022. 5
- [35] Yang Xue, Yuheng Li, Krishna Kumar Singh, and Yong Jae Lee. Giraffe hd: A high-resolution 3d-aware generative model. In *Proceedings of the IEEE/CVF Conference on Computer Vision and Pattern Recognition*, pages 18440–18449, 2022. 1, 2, 4, 5
- [36] Linjie Yang, Ping Luo, Chen Change Loy, and Xiaoou Tang. A large-scale car dataset for fine-grained categorization and verification. In *Proceedings of the IEEE conference on computer vision and pattern recognition*, pages 3973–3981, 2015. 4
- [37] Kai Zhang, Gernot Riegler, Noah Snaveley, and Vladlen Koltun. Nerf++: Analyzing and improving neural radiance fields. *arXiv preprint arXiv:2010.07492*, 2020. 2
- [38] Xuanmeng Zhang, Zhedong Zheng, Daiheng Gao, Bang Zhang, Pan Pan, and Yi Yang. Multi-view consistent generative adversarial networks for 3d-aware image synthesis. In *Proceedings of the IEEE/CVF Conference on Computer Vision and Pattern Recognition*, pages 18450–18459, 2022. 2, 5
- [39] Peng Zhou, Lingxi Xie, Bingbing Ni, and Qi Tian. Cips-3d: A 3d-aware generator of gans based on conditionally-independent pixel synthesis. *arXiv preprint arXiv:2110.09788*, 2021. 1